Dynamics of grain ejection during impact cratering in a deep dense pile.

Stéphanie Deboeuf, Philippe Gondret, Marc Rabaud

Dynamics of grain ejection during impact cratering in a deep dense pile.

S. Deboeuf
Univ. Paris 6, Univ. Paris 7, CNRS, Lab. de Physique Statistique de l'Ecole Normale Supérieure, UMR 8550, 24 rue Lhomond, 75231 Paris Cedex 05, France

P. Gondret and M. Rabaud
Univ. Paris-Sud, Univ. Paris 6, CNRS, Lab. FAST, UMR 7608, Bât. 502, Campus Univ, 91405 Orsay, France
(Dated: November 13, 2008)

The dynamics of grain ejection consecutive to a sphere impacting on a granular material is investigated experimentally and the variations of the characteristics of grain ejection with the control parameters are quantitatively studied. The time evolution of the corona formed by the ejected grains is reported, mainly in terms of its diameter and height, and favourably compared with a simple ballistic model. A key characteristic of the granular corona is that the angle formed by its edge with the horizontal granular surface remains constant during the ejection process, which again can be reproduced by the ballistic model. The energy of the ejected grains is evaluated and allows for the calculation of an effective restitution coefficient characterizing the complex collision process between the impacting sphere and the fine granular target. The effective restitution coefficient is found to be constant when varying the control parameters.

I. INTRODUCTION

Impact cratering has been recognized as an important geologic process for the last decades when the lunar craters have been finally attributed to impact structures rather than giant volcanoes as believed until 1950's [1]. The planetary impact craters such as the ones observed commonly on the Moon or the Earth result from very high energy impacts of meteorites and thus involve numerous and very complex phenomena such as shock and rarefaction wave propagation, melt and vaporization of the projectile and target materials, together with excavation by displacement and ejection of the target material [1]. In light of evidences of the discrete and sandy nature of planets surface, laboratory scale experiments of high energy impacts on granular materials were conducted [2, 3]. Since a few years, physicists have conducted laboratory scale experiments with rather low impact energy on granular matter, interesting in the crater morphology and searching for scaling laws for the crater size [4, 5, 6, 7]. Even though their energies are typically many orders of magnitude smaller than those of meteorite impacts, these small scale experiments on granular impacts may be relevant to planetary impact processes, as the progression of crater morphologies as a function of impact energy has been shown to mirror that seen in lunar craters [4]. In these impact experiments, physicists have also been interested in the penetration of the impacting sphere in the granular target [8, 9, 10, 11, 12, 13, 14]. Indeed, despite recent progress on the complex rheology of granular matter [15], the penetration dynamics of a solid sphere into a granular medium is still difficult to understand well as it involves both the complex drag resulting from frictional and collisional processes, and the final stop involving the complex "liquid/solid" transition exhibited by granular matter [16]. The penetration dynamics of the impact sphere and the grain ejection have been shown to be very different when the granular material is not dense but loose: a spectacular thin granular jet can raise very high after the impact as first demonstrated in Refs [2, 17, 18]. The effects on this granular jet of the interstitial fluid [19, 20] and of the initial packing fraction of the target [21] have then been studied. In the dense case, no granular jet but a growing granular corona is seen after the impact. These different kinds of grain ejection can be related to similar kinds of liquid ejection consecutive to the impact of a droplet into a deep or thin layer of liquid that have been first filmed by [22] and then studied extensively [23, 24]. Much less studies focusing on the grain ejection have been performed in the dense granular case: Ogale *et al.* [25] have measured the mass of the spilled-over grains and Boudet *et al.* [26] have proposed a model of ejection from the crater growth in a layer of thickness small compared to the size of both projectile and target grains at low impact velocities (~ 1 m/s), while Cintala *et al.* [27] measured ejection speeds and angles of grains at high impact velocities (~ 1 km/s). Another type of experiments concern the impact of one bead with a granular target made of the same beads [28]. Such impacts and grain ejections by an impacting projectile have been recently simulated in limiting cases, for which the impact energy is very low or very high [29, 30] or for which the projectile size is about the grains size [31, 32, 33]. We focus in the present paper on the dynamics of the granular corona formed by the ejected grains of a dense and deep pile upon low speed (~ 1 m/s) impacts. In section II, the experimental setup is described together with the measurements. A simple ballistic model is then presented in section III and compared to the experimental data. Our results are discussed within the literature in section IV. Section V ends this paper with a conclusion.

II. EXPERIMENTS

Each experimental run consists of dropping a solid sphere into a granular medium. Four different steel spheres of density ρ_s=7800 kg/m^3 are used as impactors, with different radius $R = 5.15, 6.75, 7.55, 9.50$ mm and masses M ranging thus from 4.5 g to 30 g. The steel sphere is initially hold by a magnet through a semi-spherical hole, so that the sphere can be dropped without any translational nor rotational velocity by pulling up the magnet. The sphere is released directly above the center of a container and falls along its axis. The sphere is dropped from the height h above the granular surface which is varied between 8 cm and 60 cm, and the sphere thus impacts the granular material with the velocity $V_c = \sqrt{2gh}$ (g is the acceleration of gravity) varying from 1 m/s to 4 m/s and energy $E_c = Mgh$ ranging from 3.10^{-3} J to 2.10^{-1} J. The target material consists in sieved glass beads of density $\rho_g = 2500$ kg/m^3 ($\rho_s/\rho_g = 3.1$) and mean diameter $2r = 0.4 \pm 0.1$ mm ($R/r \sim 25 - 50$), thus of mass $m = 8.10^{-5}$ g ($M/m \sim 10^4 - 10^5$). Several dimensionless numbers characterize the "strength" of the impact, among which: the Froude number based either on the projectile $V_c/\sqrt{2gR} \in [3; 9]$ or a target grain $V_c/\sqrt{2gr} \in [16; 60]$, the ratio of energy based either on the projectile $E_c/(2MgR) \in \left[10^1; 10^2\right]$ or a target grain $E_c/(2mgr) \in \left[10^7; 10^9\right]$. The granular material fills the cylindrical container of diameter 19 cm and height 26 cm. The size ratio of the container diameter over the sphere diameter is always larger than 10, so that there is no influence of the radial confinement by the lateral walls of the container neither of the bottom wall [13]. Before each drop, the granular medium is prepared by gently stirring the grains with a thin rod. The container is then overfilled and the surface levelled using a straightedge. The typical value of the solid volume fraction of the packing is 60%. Each impact experiment is lighted from the front to enhance contrast between the grains and the black background, while recorded by a high speed camera at the rate of 500 images/s and resolution of 0.16 mm/pixel. The 256 gray level images are thresholded to identify grains.

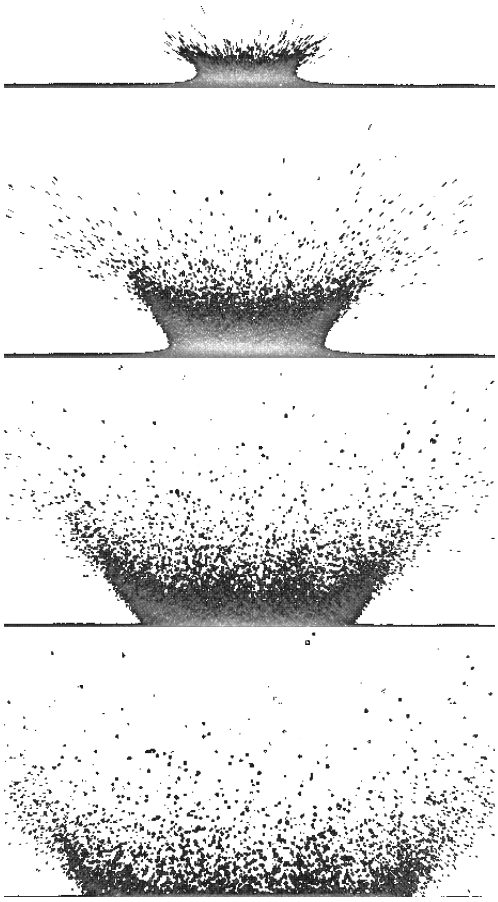

FIG. 1: Sequence of side view images separated by 30 ms, showing the typical temporal evolution of ejected grains after the impact of a steel sphere of radius $R = 6.75$ mm dropped from the height $h = 30$ cm ($V_c = 2.45$ m/s, $E_c = 0.03$ J).

Figure 1 shows a sequence of side view images separated by 30 ms illustrating the ejection dynamics of the grains after the sphere impact, defined as the time $t = 0$. One can see few isolated ejected grains above a dense corona of grains that expands radially and vertically. The amount of ejected grains can be quantified by measuring the apparent surface area A_{tot} of all the grains in each image. The evolution of A_{tot} as a function of time is reported in Fig. 2 for several experiments corresponding to different dropping heights h of the same sphere. After the impact at $t = 0$ defined as the first contact between the bottom of the sphere and the granular surface, A_{tot} increases up to a maximal value denoted $A_{tot\,max}$ at the time $t_{A_{tot\,max}}$, before decreasing. Each curve corresponds to a single impact experiment, thus without any ensemble averaging, but with a little smoothing by a slide-average over a time window of 10 ms so that no data appears before $t = 4$ ms in the reported figures. Increasing the dropping height h of a given sphere, the values $A_{tot\,max}$ and $t_{A_{tot\,max}}$ increase, accounting for the increase of both the number of ejected grains and the dynamics duration. The same goes when keeping constant the dropping height h and increasing the mass M of the impacting sphere. It is worthnoting that the exact relation between the measured apparent surface area A_{tot} of the ejected grains and the real total number of ejected grains N is not straighforward. For dilute zones of ejected grains, all the grains can be seen in the 2D images, but there is still the problem of focusing: a distant grain appears smaller than a close grain so that the grains do not have the same apparent area. The most problematic case concerns however the dense zones where some grains can be hidden by other grains.

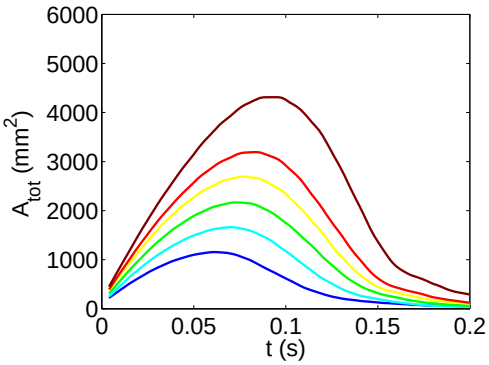

FIG. 2: (Color online) Temporal evolution of the total apparent surface of ejected grains A_{tot} for an impacting steel sphere of radius $R = 7.55$ mm dropped from different heights $h = 13$, 23, 33, 43, 48 and 58 cm (from bottom to top).

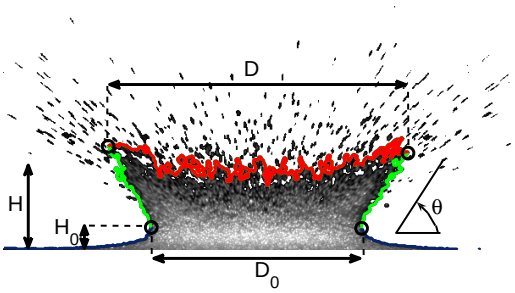

FIG. 3: (Color online) Geometrical parameters characterizing the corona of ejected grains.

Using the fact that the ejection process is axisymmetric, we can however estimate the number of ejected grains N from the measured apparent surface area A_{tot} as:

$$N = \pi N_0 / 2 A_{tot\,max} / r^2, \qquad (1)$$

where appears N_0, the number of grain by unit area in the thickness of the corona. We will see in the following that this estimation will be validated when comparing the scaling laws for N with the impact energy E_c and the corresponding scaling laws already known in the literature for the crater diameter and crater depth [7].

In impact experiments of a drop onto a liquid layer, a beautiful corona is classically observed [22, 24]. In such a liquid case, the corona is easy to define and extract as the liquid is a continuous medium. In the granular case, the corona is less easy to define as the ejected grains are individual entities. The granular corona is here defined as the largest connected part of grains in the image. We have checked that the size of the corona does not depend significantly on the lighting and contrast of the images. To investigate the time evolution of the corona and characterize its shape which is basically axisymmetrical, its contour is extracted for each image. An example of such a contour is drawn in Fig. 3. Note that this corresponds to the external contour of the ejecta curtain. This allows to detect two opposite points on the contour at the bottom (resp. at the top) of the corona as the nearest (resp. farthest) points in terms of horizontal distance. Their horizontal gap distance define respectively the minimal diameter D_0 and maximal diameter D of the corona. The height H of the corona is measured as the mean vertical position of the corona top contour between the two top points and the height of its base H_0 corresponds to the height where the corona diameter is minimal and equal to D_0. In all these height definitions, the zero is taken as the granular surface level before impact. As the corona lateral edge appears quite straight except in a small zone at the base of the corona, we extract also the angle θ formed by the corona edge with the horizontal, by a linear fit of the straight portions.

The time evolution of the corona, in terms of its height H, its maximal and minimal diameters D and D_0, and its edge slope θ, is displayed in Fig. 4 for the same experiments as in Fig. 2. The expansion of the corona is demonstrated in Fig. 4a by the increase of its height H up to a maximal value denoted H_{max} at time $t_{H_{max}}$ before decreasing. For a given sphere, H_{max} and time $t_{H_{max}}$ increase monotically with the dropping height h, so that the different curves of Fig. 4a appear in order. Note that for large impact energies (large impact heights h), H decreases to a significant non-zero value for large t values, because of the final crater rims lying above the initial free surface [4]. In the same time, the maximal diameter D and the minimal diameter D_0 increase with time, as shown in Fig. 4b and c, up to their maximal values, D_{max} and $D_{0\,max}$, when the corona disappears and its height vanishes. The evolutions of D and D_0 are different: about linear for D when parabolic for D_0. Besides, D increases significantly with the dropping height h whereas D_0 does not vary so much. Note that at the nearly end of the corona life, for vanishing height H, the values of D and D_0 become very noisy (not shown). The angle θ the corona edge forms with the horizontal, shown in Fig. 4d, is roughly constant as a function of time and whatever the dropping height h, and equal to about 56° with relative variations of $\sim 5\%$. The same kind of evolutions of all these parameters are observed for the different tested spheres.

The corona evolution reported here for granular impacts can be now compared to the corona evolution for the liquid case [24]. For the liquid case, the corona base spreads radially as the square root of time whereas it seems more close to a quadratic evolution for the granular case (see $D_0(t)$ in Fig. 4c). The scaling law of spreading is thus very different in the two granular and liquid cases, with inverse curvatures in the $D_0(t)$ plot. Besides, the angle of a granular corona is found independent of the impact velocities, as found for the liquid corona. But a big difference is that the angle of the corona depends crucially on the initial liquid thickness δ for the liquid case, as it varies from 90° for a film thickness δ larger than the drop radius R towards smaller values for smaller film thickness, e.g. $\theta \simeq 40°$ for $\delta/R = 0.1$ [23]. The fact that

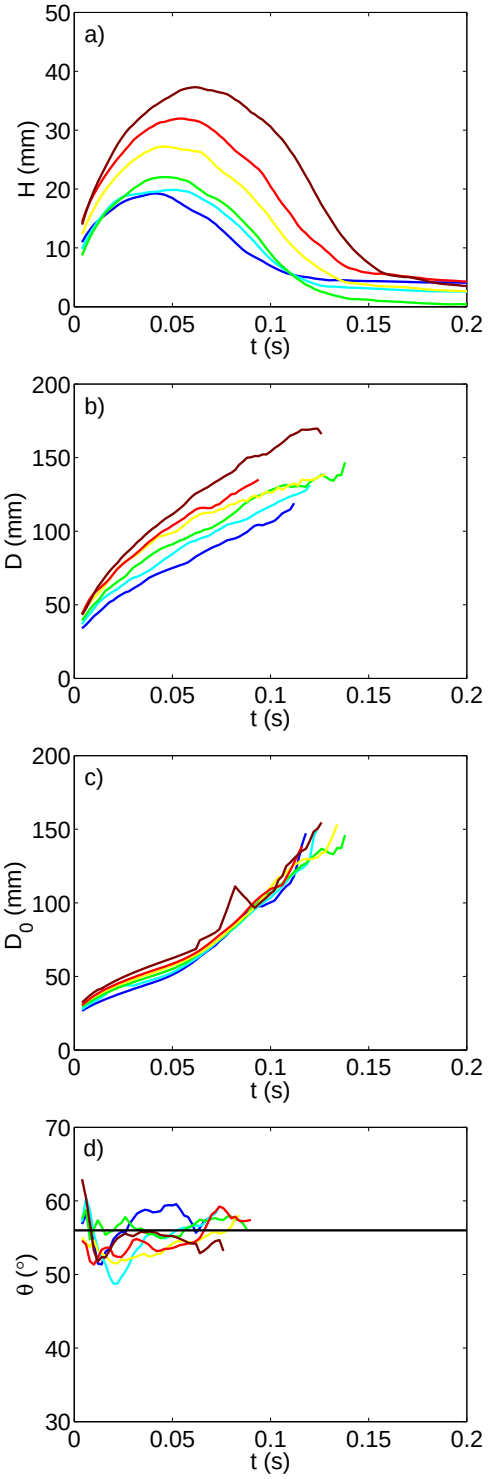

FIG. 4: (Color online) Time evolution of a) the height H, b) the maximal diameter D, c) the minimal diameter D_0, and d) the angle of the corona θ for the same experimental parameters as in Fig. 2. The horizontal line in d) is the temporal and ensemble average of $\theta(t)$ on the 65 experiments.

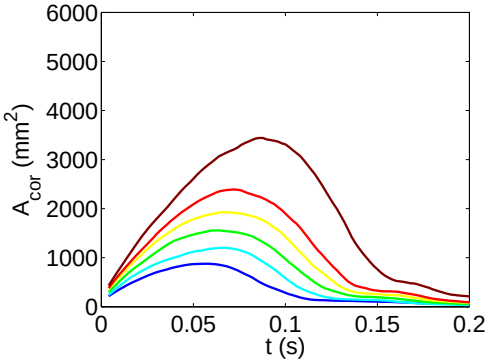

FIG. 5: (Color online) Time evolution of the apparent surface area of the corona A_{cor} for the same experimental parameters as in Fig. 2.

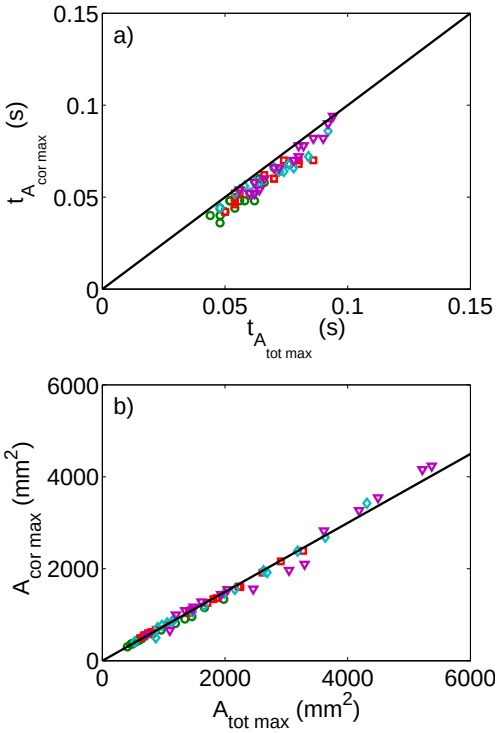

FIG. 6: (Color online) a) Time $t_{A_{cor\,max}}$ for maximal value of the corona apparent area A_{cor} as a function of time $t_{A_{tot\,max}}$ for maximal value of the total apparent area A_{tot}. The solid line is of slope 1. b) Maximal values $A_{cor_{max}}$ of A_{cor} as a function of maximal values $A_{tot_{max}}$ of A_{tot}. The solid line is a linear fit. Data symbols are for the 65 experiments with different dropping heights h for impacting spheres of radius $R = 5.15$ (○), 6.75 (□), 7.55 (◇) and 9.50 (▽) mm.

the angle of a granular corona does not seem to depend on the depth of the granular layer may be related to the collisional chains that redirected the impact velocity within a few grains layer only [32].

With the measurements of the geometrical parameters of the corona, we can now define the apparent area of the corona A_{cor}, that is related to the amount of ejected

grains contained in the corona, and compare it to the total apparent area of ejected grains A_{tot}, related to the total amount of the ejected grains, both in the corona and isolated. A_{cor} is measured as the area included inside the corona contour, which is not far from the area $H(D + D_0)/2$ corresponding to the approximate corona trapezium shape. The time evolution of A_{cor} is reported in Fig. 5 for the same experimental parameters as in Figs. 2 and 4. Even if A_{cor} is always smaller than A_{tot}, the evolution of A_{cor} is qualitatively the same as the one of A_{tot} (Fig. 2). This is confirmed by the quantitative comparison of the corresponding coordinates of the curve maxima, ($t_{A_{tot\,max}}$, $A_{tot\,max}$) and ($t_{A_{cor\,max}}$, $A_{cor\,max}$), that are reported in Fig. 6 for all the experiments (all dropping heights, all different impacting spheres). The evolutions of A_{cor} and A_{tot} are synchronized in time as illustrated by the equality $t_{A_{cor\,max}} \simeq t_{A_{tot\,max}}$ (Fig. 6a). Besides, $A_{cor\,max}$ is found proportional to $A_{tot\,max}$ with the same ratio for all experiments: $A_{cor\,max} \simeq 0.75 A_{tot\,max}$ (Fig. 6b). All this suggests that the investigation of the corona dynamics is a good first order for the study of the dynamics of grain ejection due to an impact.

Here is a summary of our main results from the evolution of the observed corona: whereas some properties, such as the dynamics duration, the maximal expansion of the corona, the number of ejected grains, depend quantitatively on the experimental parameters, some other geometrical parameters, such as the corona edge angle, its minimal diameter at its base, keep constant either for all experiments or as a function of time. How interpret these seemingly contrasting observations?

III. BALLISTIC MODEL FOR GRAIN EJECTION

Figure 1 shows that the dynamics of the grains is axisymmetric and that rapidly contact forces between grains play no role. Furthermore air friction can be estimated and is found to be negligible compared to the grain weight. Thus grain trajectory is a parabolic free flight under the action of gravity alone. Using these preliminary remarks, we now build a very simple model that reproduces the observed corona dynamics.

As a first attempt, we assume that all grains start at the same instant $t = 0$, from the same position r_0, in the same initial radial direction making an angle α with the horizontal, but with different velocity amplitudes. It is thus easy to show (Fig. 7a) that at any instant t all the grains will be located on a cone making the same angle α with a minimal radius r_1 increasing quadratically with time as $r_1(t) = r_0 + gt^2/(2\tan\alpha)$. Furthermore, if v_0 is the maximal amplitude of initial velocity, there exists at any time t a maximal radius r_2 for the cone that increases linearly with time as $r_2(t) = r_0 + v_0 \cos\alpha\, t$ and a maximal height z_2 that evolves quadratically in time as $z_2(t) = v_0 \sin\alpha\, t - gt^2/2$. These analytic results are quite similar to the dynamics observed in Fig. 1 and to the temporal evolution of the corona parameters H, D, D_0 and θ presented in Fig. 4. The hypothesis of an instantaneous release of all the grains at the same place and the same instant $t = 0$ is however clearly oversimplified. Indeed grains are emitted during a time δt of the order of the penetration time $R/V_c \sim 5$ ms and, as the projectile decelerates the emission velocity of the grains should be a decreasing function of time. On Fig. 7b, we plot the apparent cone angle $\theta(t)$ of the moving grains when released with various models of time decreasing velocities $v_0(t)$ during the time interval $\delta t = 5$ ms: a linear $[v_0(t) = v(0)(1 - t/\delta t)]$, a quadratic $[v_0(t) = v(0)(1 - t^2/\delta t^2)]$, or an exponential $[v_0(t) = v(0)\exp(-t/3/\delta t)]$ decrease with $v(0) = 1$ m/s. Except at very short times the edge angle θ remains constant and always close to the throwing angle α. While the temporal evolutions for the maximal radius r_2 and the maximal height z_2 of the apparent cone are obviously the same than for an instantaneous release, it appears to be also the same but with a delay of δt for the minimal radius r_1. As this delayed grain ejection and initial velocity decrease have no visible effect in the corona dynamics we will use in the following the simpler initial model where all the grains start at the same instant with initial velocity range $[0, v_0]$.

In the experiments we measured the time evolution of the corona parameters, i.e. the optically opaque zone formed by ejected grains, when viewed from the side. The relation between this corona that corresponds to a 2D projection of the 3D real dynamics with this latter is not straightforward. Clearly the minimal diameter D_0 and the edge angle θ are the same. Furthermore, Fig. 6 shows that the full 3D dynamics of grains and the 2D dynamics of the corona are strongly related. In the following we will then assume in the model that the height H of the compact corona is identical to the maximal height z_2 of the ballistic model and similarly we will assume that the maximal experimental diameter D of the compact corona is equal to $2r_2$. Assuming this, the temporal evolution of H, D, D_0 and θ should be given by the following set of equations:

$$H(t) = v_0 \sin\alpha\, t - gt^2/2 + H(0), \quad (2)$$

$$D(t) = D(0) + 2v_0 \cos\alpha\, t, \quad (3)$$

$$D_0(t) = D_0(0) + gt^2/\tan\alpha, \quad (4)$$

$$\theta = \alpha. \quad (5)$$

An initial height $H(0)$ has been introduced in the dynamics of $H(t)$ because in the experiment, before any grain ejection, we observe an initial swelling of the granular bed. This deformation corresponds to a plastic deformation of the substrate when the projectile starts to penetrate the bed. It may be a dilatance process that is clearly not contained in our ballistic description. The horizontal position of ejection $D(0) \approx D_0(0)$ may obviously be attributed to steric hindrance between grains and the impacting bead. Indeed, we see that $D(0)$ and $D_0(0)$ increase with the impacting sphere diameter $2R$.

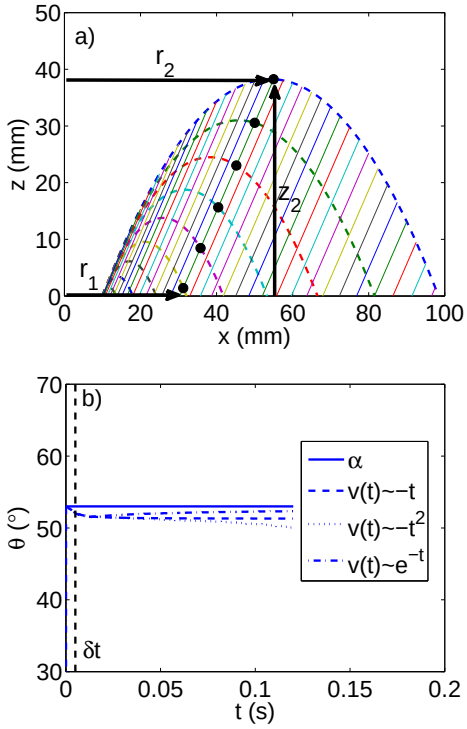

FIG. 7: (Color online) a) Ballistic model for grains ejected instantaneously from the same position in the same direction of angle α with the horizontal, with different velocity amplitudes. Trajectories are drawn in dashed lines. At any time grains align along a straight line forming the corona edge, drawn in continuous lines, of angle $\theta = \alpha$. b) Temporal evolution of the angle θ of the cone edge if grains are ejected during a finite time $\delta t = 5$ ms in the direction $\alpha = 53°$, with a linear $[v_0(t) = v(0)(1-t/\delta t)]$, quadratic $[v_0(t) = v(0)(1-t^2/\delta t^2)]$ or exponential $[v_0(t) = v(0)\exp(-t/3/\delta t)]$ decrease of ejection velocity with $v(0) = 1$ m/s.

This set of equations can be written in dimensionless form as:

$$\frac{H(t)-H(0)}{H_{max}-H(0)} = 2\left(\frac{t}{t_{H_{max}}}\right) - \left(\frac{t}{t_{H_{max}}}\right)^2, \quad (6)$$

$$\frac{D(t)}{D(0)} = 1 + \frac{2v_0\cos\alpha}{D(0)}t, \quad (7)$$

$$\frac{D_0(t)}{D_0(0)} = 1 + \frac{g}{D_0(0)\tan\alpha}t^2. \quad (8)$$

with the two scaling parameters: $t_{H_{max}} = v_0 \sin\alpha/g$ and $H_{max} = H(0) + gt^2_{H_{max}}/2$.

For each of the 65 experiments, $H(t)$ and $D(t)$ are fitted by eqs. (2) and (3) with two free parameters: $v_0 \sin\alpha$ and $H(0)$ for $H(t)$, and $v_0\cos\alpha$ and $D(0)$ for $D(t)$. Then coefficients of eq. (4) for $D_0(t)$ are deduced. The initial velocity v_0 and ejection angle α characterize the dynamical process of grain ejection induced by the impact, while $H(0)$, $D(0)$ and $D_0(0)$ are geometrical characteristics.

Figure 8 shows that when rescaled according to eqs. (6)-(7)-(8), $H(t)$, $D(t)$ and $D_0(t)$ collapse for experiments

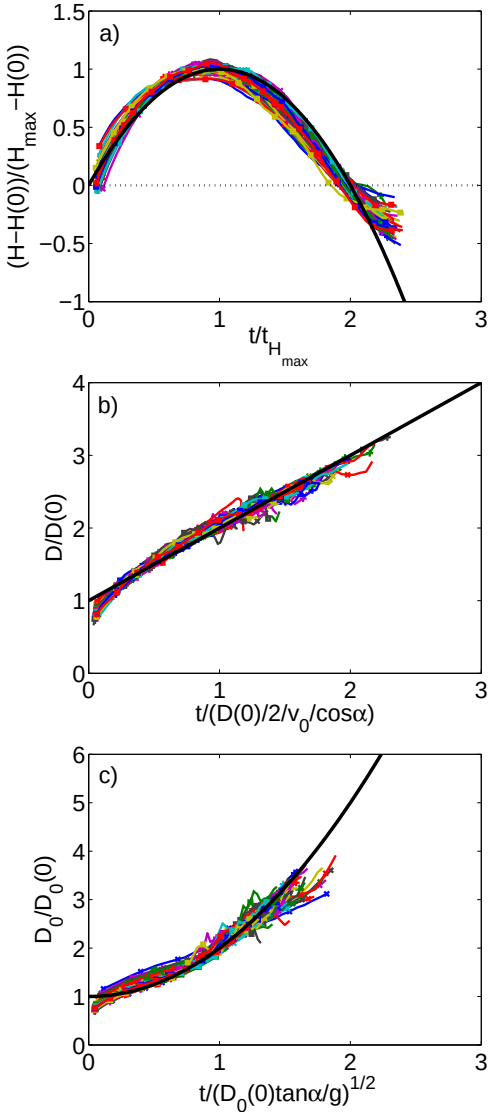

FIG. 8: (Color online) Rescaled data of a) heights $(H - H(0))/(H_{max} - H(0))$, b) top $D/D(0)$ and c) bottom diameters $D_0/D_0(0)$ as a function of rescaled time $t/t_{H_{max}}$, $t2v_0\cos\alpha/D(0)$ and $t/\sqrt{D_0(0)\tan\alpha/g}$ respectively for all of the 65 experiments, with four different sphere radius and different dropping heights.

corresponding to different dropping heights and different impacting sphere radius. These collapses confirm that the evolutions of height H and of the bottom diameter D_0 are quadratic, when the top diameter D increases linearly with time. The present scenario for grain ejection is supported by the good description of the corona dimensions as a function of time by eqs. (2)-(3)-(4) or rescaled eqs. (6)-(7)-(8), and especially by the quantitative comparison of the different angles θ and α obtained independently, as shown below.

The slope angle θ of the corona edge has been directly measured and shown to be almost constant as a function of time and for all experiments (Fig. 4d): $\theta \simeq 56° \pm 3°$.

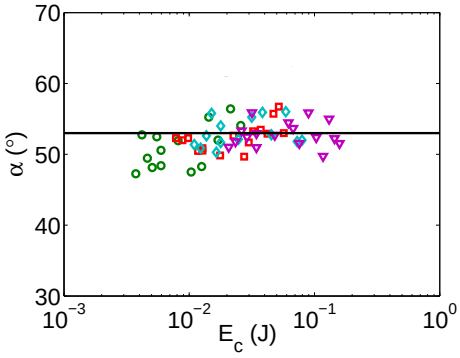

FIG. 9: (Color online) Variations of the characteristic angle of ejection α with the impact energy E_c, for the 65 experiments (same symbols as in Fig. 6).

The angle of ejection α is also found to be constant among all experiments and equal to the corona edge angle: $\alpha \simeq 53° \pm 3°$. We have checked that these angles are robustly constant for all experiments and do not depend on any impact parameter, as shown by the clear absence of any correlation of α with the impact energy E_c in Fig. 9. The equality of the angles of ejection and of the corona edge is again in favour of the present grain ejection scenario.
From eqs. (2)-(3)-(4) the area of the corona A_{cor} is calculated as:

$$A_{cor} = A_{cor}(0) + v_0 \sin\alpha D(0)t + \left(v_0^2 \sin\alpha\cos\alpha - gD_0(0)/2\right)t^2 - g^2t^4/(4\tan\alpha), \quad (9)$$

with $A_{cor}(0) = H(0)\left(D(0) + D_0(0)\right)/2$, the corona surface area at $t = 0$. This expression well describes the experimental measurements of A_{cor} (not shown) and predicts that the time of maxima for the apparent corona area $t_{A_{cor\,max}}$ is proportional to the time of maxima for its height $t_{H_{max}}$ through the coefficient 1.36.
Despite the lack of direct measurements of grains velocity, we were able to deduce a characteristic ejection velocity v_0 from our geometric measurements. Figure 10a shows the slow increase of v_0 with the impact velocity V_c, and its dependence on the sphere radius, meaning that V_c is not the relevant parameter to account for the variations of v_0. The kinetic impact energy $E_c = MV_c^2/2$ is a much better relevant parameter, as shown by Fig. 10b where the kinetic energy of one grain $mv_0^2/2$ is plotted as a function of the impact energy E_c in log-log scales. The best power law fit is:

$$mv_0^2/2 \simeq 0.56\,10^{-9}E_c^{0.37\pm0.05}, \quad (10)$$

showing a relatively small effect of the impact energy on the kinetic energy of one grain. From the ballistic model presented above and this experimental result, we can predict the variations of the total duration of the ballistic dynamics T, the maximal height H_{max} and diameter D_{max} of the corona with the impact energy E_c

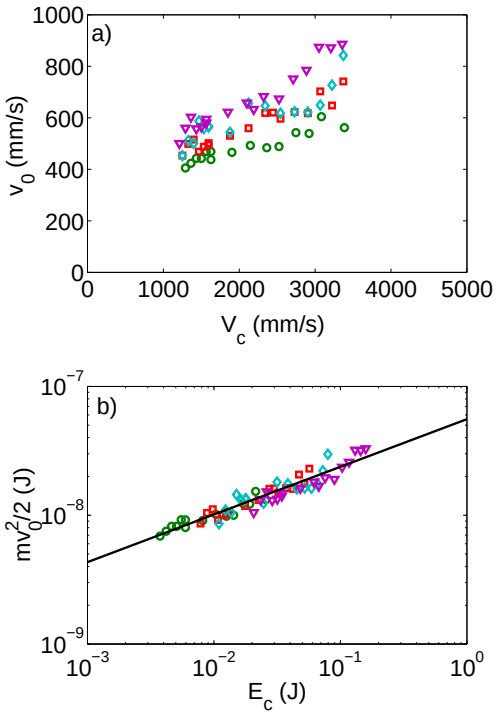

FIG. 10: (Color online) Variations of ejection parameters with the impact parameters: a) ejection velocity v_0 as a function of impact velocity V_c; b) kinetic energy of one grain $mv_0^2/2$ as a function of impact energy E_c and the best power law fit eq. (10). The symbols are the same as in Fig. 6.

as:

$$T = 2t_{H_{max}} = 2v_0 \sin\alpha/g \propto E_c^{0.19}, \quad (11)$$
$$H_{max} = gt_{H_{max}}^2/2 \propto E_c^{0.37}, \quad (12)$$
$$D_{max} = v_0^2 \sin 2\alpha/g \propto E_c^{0.37}, \quad (13)$$

allowing to characterize the duration and the extension of deposits upon an impact.
From Fig. 2, we wrote that the characteristic number of ejected grains N could be estimated from the total apparent surface of all of the ejected grains according to eq. (1). Assuming that $\pi N_0/2 \approx 1$, the number of ejected grains N is plotted as a function of the impact energy E_c in log-log scales in Fig. 11a. We see that whatever the sphere size all the experiments collapse when plotted as a function of impact energy E_c with the best power law fit:

$$N \simeq 4.8\,10^5 E_c^{0.70\pm0.05}. \quad (14)$$

We can now estimate the kinetic energy transmitted to all the ejected grains as $E_e \simeq Nmv_0^2/2$. Figure 11b shows the evolution of E_e as a function of E_c. The total kinetic energy of the grains is found proportional to the impact energy:

$$E_e \simeq 0.020E_c. \quad (15)$$

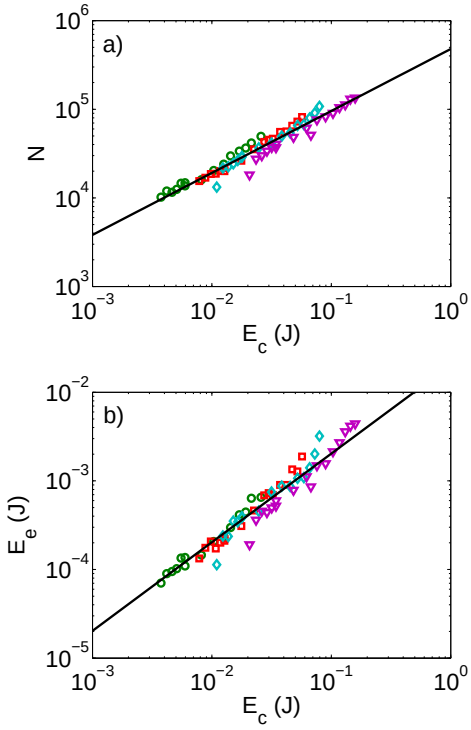

FIG. 11: (Color online) a) Number of ejected grains N as a function of impact energy E_c and the best power law fit eq. (14) for all experiments. b) Kinetic energy distributed to ejecta E_e as a function of impact energy E_c and the best power law fit eq. (15). Here N and E_e are estimated assuming $\pi N_0/2 \approx 1$. The symbols are the same as in Fig. 6.

This unexpected result allows to the definition of an effective restitution coefficient $\rho = \sqrt{E_e/E_c} \approx 0.14$. The small value of ρ confirms the well known and well used fact that granular beds are very efficient dissipating systems.

To summarize, except at the time of impact when a slight global displacement of the granular surface layer occurs, all the geometrical parameters of the corona formed by ejected grains are well described by a very simple ballistic model, showing no effect of any inter-grains interactions on the dynamics.

IV. DISCUSSION

When varying the dropping height and the size of the impacting sphere, the impact energy appears to be the relevant parameter to describe the variations of ejection properties, as observed for the crater size scaling laws [4, 5, 6, 7] and for the ejection properties when the projectile and the target material are composed of the same beads [28]. As qualitatively observed in [25], more energetic is the impact and more grains are ejected. Moreover grains are ejected with higher velocities. However, the dependence on impact energy of ejection velocity is smoother than that of the number of ejected grains. In the configuration of [28], the impact induces the rebound of the projectile and the ejection of some grains only, so that an extensive number of experiments are realized to do ensemble averages, leading to statistical distributions of ejection velocity, angle and number of ejected grains. Despite the different phenomenology and the different ratio of projectile over target grain sizes ($R/r = 1$ in [28] and $R/r \sim 25-50$ here), the variations of ejection properties with impact energy are close: $\overline{v_0} \propto E_c^{0.12}$ and $\overline{N} \propto E_c^{0.75}$ in [28], while $v_0 \propto E_c^{0.19}$ and $N \propto E_c^{0.70}$ here, where $\overline{v_0}$ and $\overline{N}$ refer to averaged quantities of ejection velocity and number of ejected grains. This may suggest that the present scaling laws hold whatever the ratio R/r, that would need still to be verified.

By contrast with the previous discussed characteristics, the direction of ejection appears to be constant when varying the dropping height of the impacting sphere and its radius, and equal to about $\approx 55°$. This independence and this value agree with results observed both in the case of high speed impacts, for which experiments of sphere/sand impacts [27] and simulations of sphere/spheres impacts [30] found values between 40° and 60°; and in the case of low speed impact of a sphere with identical spheres, for which experiments found on average 60° [28].

All the geometrical properties of the corona formed by the ejected grains have been well described by a simple ballistic model, supporting that grains are quasi-instantaneously ejected at time of impact from the same place in a constant direction. This model can be compared with the one presented in [26], that allows to describe the time exponential growth of the crater in a very thin granular layer. In both ejection models, grains are ejected in a constant direction but with different velocity amplitudes. But the essential difference is the spatial extension of the places of ejection: whereas ejection is assumed to be localized in our model, it is assumed to be spatially extended in [26]. In the later case, this leads to a corona edge, which slope is not constant as a function of time, but decreases from values around 180° to 90°.

Our estimation of the number of ejected grains N can be compared with the volume of craters lying at the surface after an impact from the experimental results of [7]. By accurately characterizing the whole shape of craters by laser profilometry, they found that craters have nearly hyperbolic profiles:

$$z(r,\phi) = z_c + \sqrt{b^2 + c^2 r^2}, \tag{16}$$

with (z, r, ϕ) the cylindrical coordinates. The parameters (z_c, b, c) can be related to $(H_{fit}, R_{fit}, c_{fit})$, that characterize respectively the depth, the radius and the slope of the crater and are found to scale with the experimental parameters (see [7]). From eq. (16), the volume V of craters can be calculated as:

$$V = \frac{\pi}{3} H_{fit} R_{fit}^2 \left(1 + \frac{b}{H_{fit} + 2b}\right), \tag{17}$$

showing the obvious scaling $V \propto H_{fit}R_{fit}^2$, with a correction factor. Based on the scaling laws found in [7], Fig. 12a shows the simple scaling of the crater volume V with the impact energy E_c despite a light effect of the projectile radius R:

$$V \simeq 3.6\,10^4 E_c^{0.67}. \quad (18)$$

The power law exponents of V eq. (18) and N eq. (14) with E_c are nearly the same (respectively 0.67 and 0.70), that definitely confirms that the geometrical measurements made on the corona give relevant and quantitative information on the grain ejection dynamics. The above comparison allows also for the exact determination of the factor $\pi N_0/2$ in eq. (1) as $(V\Phi)/(N4/3\pi r^3)$, with the solid volume fraction $\Phi = 0.60$: Fig. 12b shows that $\pi N_0/2$ is almost constant for all experiments and equal to 1.5, that is not far from the value of 1 assumed for the previous calculations of N and E_e. This means that the previous values of N and E_e reported on Fig. (11) have to be multiplied by a factor of 1.5 to be even more precise.

The above scalings for crater volume eq. (18) and number of ejected grains eq. (14) with impact energy are compatible with the following simple argument based on the crucial role of gravity in the crater excavation and grain ejection, often made to derive scaling laws for crater dimensions [1, 4, 5]: the available energy goes into lifting a volume V by a distance $V^{1/3}$ against gravity leading to $V \propto E_c^{0.75}$. By contrast, if the target material strength dominates, the available energy would be dissipated by plastic flow of the medium throughout a volume V leading to $V \propto E_c$.

The energy of the ejected grains is finally evaluated and allows for the calculation of an effective coefficient of restitution characterizing the complex collision process between the impacting sphere and the fine granular target. An important result is that the effective restitution coefficient is almost constant when varying the control parameters, and is estimated to $\sqrt{0.02 * 1.5} = 0.17$ after the light correction made to $\pi N_0/2$. However this value is certainly dependent on the initial solid volume fraction of the granular target, that would be interesting to study in details. This allows to quantify the energy transmitted to the ejected grains: $2\% * 1.5 = 3\%$ (after the light correction made to $\pi N_0/2$) of the initial available energy is transmitted to the grains through their ejection, whereas only a tiny fraction $(0.1 - 0.5\%$ according to [7]) is required to excavate the crater, for the grains to move just above the granular surface layer but with 0 velocity. One rough illustration of the significance of the kinetic energy of ejected grains compared with the potential energy of the crater lies in the larger values of the maximal height of the corona $H_{max} \in [10\ mm; 40\ mm]$ (see Fig. 4a) than the depth of craters $\in [4\ mm; 10\ mm]$ [4, 7] for the same materials and conditions of impacts. This shows that on one hand the kinetic energy of the ejected grains has to be taken into account when balance of energies are considered, and on the other hand it keeps small compared to the 97% of impact energy that is transmitted to the granular target for it to deform and dissipated through frictional contacts and inelastic collisions.

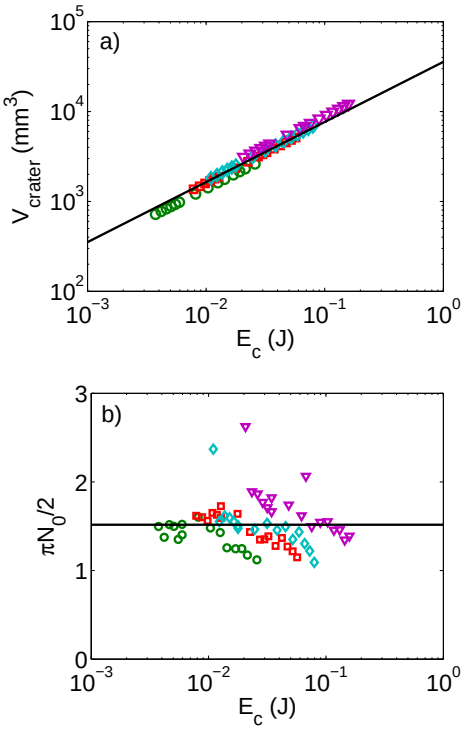

FIG. 12: (Color online) a) Scaling law for crater volume V according to eq. (17) and from experimental results in [7] as a function of impact energy E_c and for the different projectile radius R used here. The solid line is the best power law fit eq. (18). b) Correction factor $\pi N_0/2$ (instead of 1 as assumed here) deduced from the comparison of the number of ejected grains N estimated here from eq. (1) with the crater volume V. The symbols are the same as in Fig. 6.

V. CONCLUSION

The dynamics of grain ejection due to a large impacting sphere on a granular material has been experimentally investigated through the time evolution of the corona formed by the ejected grains, in terms of its geometrical evolution. Whereas the dimensions of the corona - its height, top and bottom diameters- change with time, the angle formed by its edge with the horizontal granular surface remains constant during the ejection process. All these geometrical properties are well described by a simple ballistic model, supporting that grains are quasi-instantaneously ejected at time of impact from the same position in a constant direction. This direction appears to be constant when varying the dropping height of the impacting sphere and its radius, and equal to about 55°. One may wonder how changes this angle with the shape of the impacting projectile. By contrast, the typical ejection velocities and number of ejected grains change when

varying experimental parameters and are controlled by the impact energy through power laws. The energy of the ejected grains is finally evaluated and allows for the calculation of an effective coefficient of restitution characterizing the complex collision process between the impacting sphere and the fine granular target. An important result is that the effective restitution coefficient is constant when varying the control parameters.

[1] H.J. Melosh, Impact cratering: a geologic process (Oxford University Press, New York, 1989).

[2] M.A. Cook and K.S. Mortensen, Impact cratering in granular materials, J. Appl. Phys. **38**, 13 (1967).

[3] S. Yamamoto, K. Wada, N. Okabe and T. Matsui, Transient crater growth in granular targets: an experimental study of low velocity impacts into glass sphere targets, Icarus **183**, 215-224 (2006).

[4] A.M. Walsh, K.E. Holloway, P. Habdas and J.R. de Bruyn, Morphology and scaling of impact craters in granular media, Phys. Rev. Lett. **91**, 104301 (2003).

[5] J.S. Uehara, M.A. Ambroso, R.P. Ojha and D.J. Durian, Low-speed impact craters in loose granular media, Phys. Rev. Lett. **90**, 194301 (2003).

[6] X.J. Zheng, Z.T. Wang and Z.G. Qiu, Impact craters in loose granular media, Eur. Phys. J. E **13**, 321-324 (2004).

[7] S.J. de Vet and J.R. de Bruyn, Shape of impact craters in granular media, Phys. Rev. E **76**, 041306 (2007).

[8] J.R. de Bruyn and A.M. Walsh, Penetration of spheres into loose granular media, Can. J. Phys. **82**, 439-446 (2004).

[9] M.P. Ciamarra, A.H. Lara, A.T. Lee, D.I. Goldman, I. Vishik and H.L. Swinney, Dynamics of drag and force distributions for projectile impact in a granular medium, Phys. Rev. Lett. **92**, 194301 (2004).

[10] M.A. Ambroso, C.R. Santore, A.R. Abate and D.J. Durian, Penetration depth for shallow impact cratering, Phys. Rev. E **71**, 051305 (2005).

[11] M. Hou, Z. Peng, R. Liu, K. Lu and C.K. Chan, Dynamics of a projectile penetrating in granular systems, Phys. Rev. E **72**, 062301 (2005).

[12] H. Katsuragi and D.J. Durian, Unified force law for granular impact cratering, Nature Physics **3**, 420-423 (2007).

[13] A. Seguin, Y. Bertho and P. Gondret, Influence of confinement on granular penetration by impact, Phys. Rev. E **78**, 010301 (2008).

[14] D.I. Goldman and P. Umbanhowar, Scaling and dynamics of sphere and disk impact into granular media, Phys. Rev. E **77**, 021308 (2008).

[15] G.D.R. Midi, On dense granular flows, Eur. Phys. J. E **14**, 341-365 (2004).

[16] S. Deboeuf, E. Lajeunesse, O. Dauchot and B. Andreotti, Flow rule, self-channelization, and levees in unconfined granular flows, Phys. Rev. Lett. **97**, 158303 (2006).

[17] S.T. Thoroddsen and A.Q. Shen, Granular jets, Phys. Fluids **13**, 4-6 (2001).

[18] R. Mikkelsen, M. Versluis, E. Koene, G.-W. Bruggert, D. van der Meer, K. van der Weele, and D. Lohse, Granular Eruptions: Void Collapse and Jet Formation, Phys. Fluids **14**, S14 (2002).

[19] J.R. Royer, E.I. Corwin, P.J. Eng and H.M. Jaeger, Gas-mediated impact dynamics in fine-grained granular materials, Phys. Rev. Lett. **99**, 038003 (2007).

[20] G.A. Caballero Robledo, R.P. Bergmann, D. van der Meer, A. Prosperetti and D. Lohse, Role of Air in Granular Jet Formation, Phys. Rev. Lett. **99**, 018001 (2007).

[21] J.O. Marston, J.P.K. Seville, Y-V. Cheun, A. Ingram, S.P. Decent, and M.J.H. Simmon, Effect of packing fraction on granular jetting from solid sphere entry into aerated and fluidized beds, Phys. Fluids **20**, 023301 (2008).

[22] A.M. Worthington, A study of splashes, (Longmans, Green, and Co., London, 1908).

[23] A.I. Fedorchenko and A.-B. Wang, The formation and dynamics of a blob on free and wall sheets induced by a drop impact on surfaces, Phys. Fluids **16**, 3911-3920 (2004).

[24] A.L. Yarin, Drop impact dynamics: splashing, spreading, receding, bouncing, Ann. Rev. Fluid Mech. **38**, 159-192 (2006).

[25] S.B. Ogale, S.R. Shinde, P.A. Karve, A.S. Ogale, A. Kulkarni, A. Athawale, A. Phadke and R. Thakurdas, Impact-induced splash and spill in a quasi-confined granular medium, Physica A **363** 187-197 (2006).

[26] J-F. Boudet, Y. Amarouchene and H. Kellay, Dynamics of impact cratering in shallow sand layers, Phys. Rev. Lett. **96**, 158001 (2006).

[27] M.J. Cintala, L. Berthoud, and F. Horz, Ejection-velocity distribution from impact into coarse-grained sand, Meteor. Planet. Sci. **34**, 605-623 (1999).

[28] D. Beladjine, M. Ammi, L. Oger and A. Valance, Collision process between an incident bead and a three-dimensional granular packing, Phys. Rev. E **75**, 061305 (2007).

[29] L.S. Tsimring and D. Volfson, Modeling of impact cratering in granular media, in Powders and Grains (A. A. Balkema Publishers, Stuttgart, 2005), pp 1215-1218.

[30] K. Wada, H. Senshu and T. Matsui, Numerical simulation of impact cratering on granular material, Icarus **180**, 528-545 (2006).

[31] L. Oger, M. Ammi, A. Valance and D. Beladjine, Discrete element method studies of the collision of one rapid sphere on 2D and 3D packings, Eur. Phys. J. **17**, 467-476 (2005).

[32] J. Crassous, D. Beladjine and A. Valance , Impact of a projectile on a granular medium described by a collision model, Phys. Rev. Lett. **99**, 248001 (2007).

[33] F. Bourrier, F. Nicot and F. Darve, Physical processes within a 2D granuler layer during an impact, Granular Matter **10**, 6 (2008).